BLIND SPATIAL UNMIXING OF MULTISPECTRAL IMAGES: AN APPROACH BASED ON TWO-SOURCE SPARSITY AND GEOMETRICAL PROPERTIES

Djaouad Benachir[1,2,3]*, Yannick Deville*[1]*, Shahram Hosseini*[1]

[1] IRAP, Université de Toulouse (UPS-OMP-CNRS), 14 av. Edouard Belin, 31400 Toulouse, France.
[2] Agence Spatiale Algérienne (ASAL), 14 rue Omar Aissaoui, Algiers, Algeria.
[3] IRIT, Université Paul Sabatier, 118 Route de Narbonne, 31062 Toulouse, France.
{Djaouad.Benachir, Yannick.Deville, Shahram.Hosseini} @irap.omp.eu

ABSTRACT

Due to the limited spatial resolution of some remote sensing sensors, their image pixel spectra are commonly mixtures of elementary contributions. To analyze this type of images, it is necessary for some applications to perform spectral unmixing. This procedure allows the decomposition of a mixed pixel spectrum into a set of pure material spectra, and a set of abundance fractions. To this end, we here propose a new unsupervised spatial Blind Source Separation approach based on sparsity and geometrical properties. This approach first consists in finding small zones (composed of several adjacent pixels) containing only two sources using a spatial correlation-based method. This stage is followed by an identification stage where we geometrically estimate the pure material spectra. The final stage is the estimation of the searched abundances using a non-negative least squares method. The results obtained for simulated mixtures of realistic sources show the good performance of our method.

Index Terms— Blind Source Separation, Sparse Component Analysis, spectral unmixing, multispectral images.

1. INTRODUCTION

In space remote sensing, image pixel spectra are commonly mixtures of elementary contributions (pixels of the data contain contributions from more than one pure material). To analyze such images, it is often necessary to perform spectral unmixing. This procedure allows the decomposition of a mixed pixel spectrum into a set of pure material spectra (called endmembers) and a set of abundance fractions showing the ratio of each endmember in each pixel. To achieve this goal, we can find in the literature a variety of methods that can be classified into three main categories: geometrical, statistical and sparse [1, 2]. Among these methods, many are related to the Blind Source Separation (BSS) problem, which permits the estimation of a set of unknown source signals from a set of observed signals supposed to be mixtures of these source signals [3, 4, 5]. Most unmixing methods are applied to *hyperspectral* remote sensing images which have the advantage of providing a large amount of spectral information. On the contrary, few of them can be used for *multispectral* images because of the limited number of spectral bands with regard to the number of sources present in the image [6, 7, 8, 9, 10].

Various sparsity-based BSS methods have been developed, either in the temporal analysis space, or the time-frequency or even time-scale spaces (see [11, 12, 13, 14] and in particular [15, 16, 17]). Recently, in [18] the same type of approach as in [15] has been applied to multispectral space images. To be applicable, this method needs a sparsity hypothesis: for each pure material, the multispectral image must contain a *single-source* spatial zone (composed of several adjacent pure pixels) where only this material is present.

The sparsity hypothesis upon which this method rests is unfortunately not applicable to certain remote sensing images whose spatial resolution is too low for them to contain pure pixels and therefore all the necessary single-source zones for the estimation of each of the sources. This prompted us to work with a less restrictive assumption that is the presence of some "two-source zones" (zones containing only two pure materials). In this paper, we propose a new BSS method for multispectral images, which are more difficult to unmix than hyperspectral images, as explained above. This method is based on the detection of two-source zones for the identification of endmembers. These estimated spectra are then used to unmix each image pixel using a least squares method with non-negativity and sum-to-one constraints, and therefore to estimate the searched abundance fractions.

In the second section of this paper, we present the used mixing model as well as some properties on which our approach is based. The method is detailed in Section 3. In Section 4, we present some test results before proceeding to the conclusion in Section 5.

2. DATA MODEL AND PROPERTIES

2.1. Mixing model

We assume that each incident radiation interacts with a single type of material, which implies a linear mixing model [1]. In this case, after vectorizing the spatial dimensions, one can express the non-negative observed reflectance in the ℓ^{th} band from a given pixel n as follows:

$$x_\ell(n) = \sum_{m=1}^{M} r_{\ell m} f_m(n) \quad \forall n = \{1 \cdots N\}, \ell = \{1 \cdots L\}, \quad (1)$$

where $r_{\ell m}$ is the ℓ^{th} component of the m^{th} endmember, $f_m(n)$ represents the abundance fraction of the m^{th} pure material in the n^{th} pixel, and M is the number of pure materials.

If one considers the N pixels of a multispectral image composed of L spectral bands, one gets the following matrix expression: $X = RF$, where X is the $(L \times N)$ observed multispectral image, the columns of R contain the endmembers and each column of F contains the abundance fractions of all pure materials in the considered pixel. In addition, these data meet the following non-negativity and sum-to-one constraints:

$$f_m(n) \geq 0, r_{\ell m} \geq 0 \quad \text{and} \quad \sum_{m=1}^{M} f_m(n) = 1. \quad (2)$$

The authors would like to thank M. Cadilhac from Aix-Marseille University (France), for helpful discussions regarding this work.

According to the BSS terminology, the abundance fraction matrix F and the endmember matrix R will hereafter be respectively called source and mixing matrices. Given an observation matrix X, we aim to estimate the matrices R and F.

2.2. Data properties

In the proposed approach, we first focus on pixels containing only two sources with indices i and j ($i \neq j$), among all the M sources considered in the image data. Due to Eq. (1), each such pixel (called "two-source pixel" hereafter) reads as:

$$x_\ell(n) = r_{\ell i} f_i(n) + r_{\ell j} f_j(n). \quad (3)$$

Considering Eq. (3), and taking into account $f_j(n) = 1 - f_i(n)$ (due to Eq. (2)), we obtain:

$$x_\ell(n) = f_i(n)[r_{\ell i} - r_{\ell j}] + r_{\ell j}. \quad (4)$$

If we now use two spectral bands with indices ℓ and p ($\ell \neq p$), we obtain for each pixel n a couple of values ($x_\ell(n)$,$x_p(n)$) defining a point in the (x_ℓ, x_p) plane. The set of two-source pixels defines a scatter plot in this plane, and we therefore want to analyse the shape of this scatter plot. Given Eq. (4), we have:

$$x_\ell(n) - r_{\ell j} = f_i(n)[r_{\ell i} - r_{\ell j}] \quad (5)$$
$$x_p(n) - r_{pj} = f_i(n)[r_{pi} - r_{pj}], \quad (6)$$

which yields:

$$f_i(n)[r_{pi} - r_{pj}][x_\ell(n) - r_{\ell j}] = f_i(n)[r_{\ell i} - r_{\ell j}][x_p(n) - r_{pj}]. \quad (7)$$

Eq. (7) defines a straight line in the (x_ℓ, x_p) plane. Therefore, let us assume that only two sources $f_i(n)$ and $f_j(n)$ are not null everywhere in a spatial zone composed of adjacent pixels (this is called a "two-source analysis zone" hereafter). Then, all corresponding points ($x_\ell(n)$,$x_p(n)$) belong to the above-defined line (7). On the contrary, if more than two sources are non-zero and vary arbitrarily in a zone, the corresponding points are not on a line. The two-source line (7) may also be defined by the expression of the 2^{nd} point coordinate with respect to the 1^{st} one, as follows:

$$x_p(n) = a x_\ell(n) + r_{pj} - a r_{\ell j}, \quad (8)$$

with: $a = \dfrac{r_{pi} - r_{pj}}{r_{\ell i} - r_{\ell j}}$ and $r_{\ell i} \neq r_{\ell j}$.
In addition, the points only belong to a segment of this line, since $0 \leq f_i(n) \leq 1$. The ends of this segment are therefore defined by:
(1) $f_i(n) = 0$:
In this case, we obtain from Eq. (5) and (6), $x_\ell(n) = r_{\ell j}$, and $x_p(n) = r_{pj}$. This is normal, because only source j is present, and it's its spectrum that is observed in such a pixel.
(2) $f_i(n) = 1$:
In this case $x_\ell(n) = r_{\ell i}$, and $x_p(n) = r_{pi}$.

If we now suppose that there exists in the considered image, at least one two-source analysis zone for each pair of sources (among the M sources in the considered image), then we obtain a straight line for each possible pair of sources. We have a total of $\frac{M(M-1)}{2}$ possible line segments. These segments have common extremities corresponding to the M sources. Each of these extreme points has the following coordinates: $[r_{\ell m}, r_{pm}]$ ($m = \{1 \cdots M\}$).
Figure 1 shows a scatter plot obtained for pixels corresponding to all pairs of sources selected from an overall set of 4 sources. As mentioned above, this implies 6 possible lines.

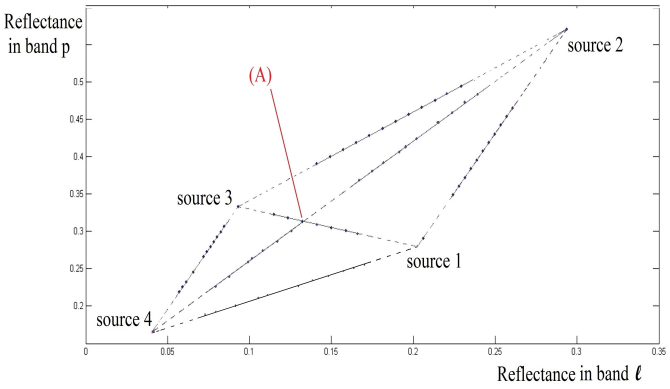

Fig. 1. $2D$ scatter plot corresponding to two-source pixels

The most difficult case and the one that interests us is when the points associated with each pair of sources do not cover the whole of each possible segment, particularly its extremities, which correspond to pure pixels (see dotted line connecting two line segments in Figure 1). In this paper, pure pixels are therefore ignored (i.e. they do not exist, or single-source zones are detected e.g. using the method from [18] and they are skipped). In this case, assume we have succeeded in estimating two lines corresponding to two pairs of sources, with indices $[i, j]$ for the first pair and $[j, k]$ for the second one (with $i \neq k$). Assuming these lines are not identical (still for two spectral bands), then we can estimate (for each line), **(1)** their slopes and **(2)** their intercepts. This allows us to deduce *their intersection point* and thus obtain the coordinates $[r_{\ell j}, r_{pj}]$, corresponding to the j^{th} endmember.
The above analysis considering only two spectral bands is useful to understand the preliminary version of our approach. However, using only two bands does not allow us to completely solve the problem: on the one hand, the obtained intersection points for all pairs of sources only give us the part of the spectra corresponding to these two spectral bands (among the L bands considered in the image). On the other hand, these 2D scatter plots also include spurious line intersections, i.e. intersections between fully disjoint pairs $[i, j]$ and $[i', j']$ of sources, which do not correspond to actual endmembers (see point A in Figure 1). Blindly determining all line intersections would therefore lead to spurious endmembers. This problem results from the fact that two (non-parallel) lines always intersect in the 2D space. To solve it, we now extend our approach to $L > 2$ spectral bands. To this end, it is first necessary to estimate the parameters of the L-dimensional-space lines associated with each two-source zone, to classify these parameters, to determine the intersection points which provide spectra estimates, and finally to estimate the abundance maps. This is detailed below.

3. PROPOSED UNMIXING METHOD

From the above-discussed properties, we propose a new BSS method for multispectral remote sensing images. This method is based on the detection of **two-source** zones (spatial zones containing only two sources), classification and some geometrical tools.

3.1. Two-source zone detection stage

Multispectral images are firstly divided into small adjacent or overlapping spatial zones, denoted by ψ (analysis zones). Each two-dimensional zone consists of adjacent pixels: for example, we can choose 5 pixel $\times$ 5 pixel zones. These analysis zones are then explored to determine the ones where only two pure materials are present. For such sought *two-source zones*, using the zero-mean versions of the observed signal in bands ℓ and p, Eq. (5) and (6) yield:

$$\bar{x}_\ell(n) = (r_{\ell i} - r_{\ell j})\bar{f}_i(n) \tag{9}$$

$$\bar{x}_p(n) = (r_{pi} - r_{pj})\bar{f}_i(n), \tag{10}$$

with $\bar{x_\ell} = x_\ell - \mu_{x_\ell}$ and $\bar{f}_i = f_i - \mu_{f_i}$ (μ_{x_ℓ} and μ_{f_i} represent the means of x and f_i over the considered analysis zone).
We can therefore deduce from Eqs. (9) and (10) , that $\bar{x}_\ell(n)$ et $\bar{x}_p(n)$ vary *proportionally* over two-source zones.
For each analysis zone, we detect the above proportionality by calculating the **cross-correlation coefficients** $\rho_{x_\ell x_p}(\psi)$, between the centred observed signals in bands ℓ and p, defined as follows:

$$\rho_{x_\ell x_p}(\psi) = \frac{\langle \bar{x_\ell}(\psi), \bar{x_p}(\psi)\rangle}{\|\bar{x_\ell}(\psi)\| \cdot \|\bar{x_p}(\psi)\|} \quad \forall \ell, p = \{1 \cdots L\}\,,\ and\ \ell > p, \tag{11}$$

where the column vector $\bar{x_\ell}(\psi)$ contains all centred pixel values $\bar{x_\ell}(n)$ in the considered analysis zone ψ. $\|x\|$ and $\langle x, y\rangle$ respectively represent the 2-norm of x and inner product of x and y.
Applying the Cauchy-Schwarz inequality to Eq. (11), shows that: $|\rho_{x_\ell x_p}(\psi)| \leq 1$, $\forall \ell, p = \{1 \cdots L\}$ and $\ell > p$, with equality if and only if $\bar{x_\ell}(\psi)$ and $\bar{x_p}(\psi)$ are linearly dependent.
Then, if in the considered zone, the number of materials is **equal to two**, $|\rho_{x_\ell x_p}(\psi)|$ is high (ideally equal to one). Now, in zones where more than two sources yield non-zero vectors $\bar{f}_i(\psi)$, all $|\rho_{x_\ell x_p}(\psi)|$ are significantly lower than one under mild assumptions[1].
In practice, for each zone, we calculate the minimum among $|\rho_{x_\ell x_p}(\psi)|$ (for all ℓ, p with $\ell > p$). If this measure is greater than a threshold (experimentally set to 0.996 in our tests), we consider this zone as being a **two-source zone**.

3.2. Identification stage

This important stage consists in estimating the columns of the mixing matrix. To achieve this goal, we first estimate the L-dimensional line parameters related to each two-source zone supposedly present in the considered data (Part I), then we classify all these estimated parameters which permit us to identify a *single* line associated with each pair of sources (Part II). Finally, we calculate the minimum distance between such lines and obtain the coordinates of the searched endmembers in the L-dimensional space (Part III).

3.2.1. Part I: Line parameter estimation

To estimate the parameters of a straight line in an L-dimensional space, we use the following approach. Consider a line D represented by the following parametric equation [19, 20]:

$$\mathbf{p}_s = s\mathbf{u} + \mathbf{d}, \tag{12}$$

with $\mathbf{p}_s$, $\mathbf{u}$ and $\mathbf{d}$, L-dimensional column vectors and s a scalar.
We want to estimate $\mathbf{u}$ and $\mathbf{d}$ to minimize the mean-squared error between the data points (corresponding to pixels in the considered two-source zone) and the generated line. Each analysis zone yields a matrix $X(\psi)$ containing the pixel values $x_\ell(n)$ of the considered analysis zone, in column ℓ (with $\ell = \{1 \cdots L\}$). One of the possible solutions for fitting a line to data points is to determine the first principal axis of these data. To this end, we use the following estimate [19, 20]:
(1) $\mathbf{d}$ = *mean of the columns of* $X^T(\psi)$, corresponding to the center of gravity of these data (where ^{T} stands for transpose).
(2) $\mathbf{u}$ = eigenvector associated with the largest eigenvalue of the covariance matrix of $X(\psi)$.
However, when fitting a model to data, it is important that there are no mutually dependent (redundant) parameters in this model. Otherwise, the solution of the fitting procedure is not unique. In Eq. (12), the line is defined by $2L$ parameters, i.e., the components of $\mathbf{u}$ and $\mathbf{d}$. However, this overspecifies the line because a line in an L-dimensional space can be defined by $2L - 2$ parameters as follows, provided it is not orthogonal to the first axis, i.e. provided the first component u_1 of $\mathbf{u}$ is non-zero. Components 1 and ℓ of Eq. (12) read:

$$p_1 = su_1 + d_1 \text{ and } p_\ell = su_\ell + d_\ell, \text{ with } \ell = \{2 \cdots L\}\,.$$

From this we obtain: $\dfrac{p_1 - d_1}{u_1} = \dfrac{p_\ell - d_\ell}{u_\ell} = s,$

which yields: $p_\ell = \dfrac{u_\ell}{u_1}p_1 + d_\ell - \dfrac{u_\ell}{u_1}d_1,$

that is:

$$p_\ell = {u_\ell}^* p_1 + {d_\ell}^*, \tag{13}$$

where the $2L - 2$ normalized parameters are defined as:

$${u_\ell}^* = \frac{u_\ell}{u_1} \text{ and } {d_\ell}^* = d_\ell - \frac{u_\ell}{u_1}d_1. \tag{14}$$

Eq. (13) and (14) also apply to $\ell = 1$, by introducing ${u_1}^* = 1$ and ${d_1}^* = 0$. Gathering all L components ${u_\ell}^*$ (resp. ${d_\ell}^*$) in a vector $\mathbf{u}^*$ (resp. $\mathbf{d}^*$), Eq. (13) defining the considered line may be written in vector form as:

$$\mathbf{p}_{s^*} = s^*\mathbf{u}^* + \mathbf{d}^*, \quad \text{with } s^* = p_1.$$

For the sake of readability, s^* is denoted as s in Section 3.2.3.

3.2.2. Part II: Classification of line parameter vectors

For each pair of sources, the above part yields several couples of vectors $\mathbf{u}^*$ and $\mathbf{d}^*$, i.e. one couple for each analysis zone only containing these two sources. We then aim at deriving a *single* couple $(\mathbf{u}^*, \mathbf{d}^*)$ for each pair of sources. To this end, we re-arrange each estimated couple $(\mathbf{u}^*, \mathbf{d}^*)$ as an overall vector and we classify these vectors by successively using each of them as follows. After setting the first vector to a first class denoted by "class-1", each vector is compared to this class by computing the distance between them, i.e. the 2-norm of their difference. Whenever this distance is less than a threshold (experimentally set to 10^{-4} in our tests), we assign the tested vector to the first class. Otherwise, we create a new class ("class-2") and assign this vector to it. Then, we compare the subsequent vectors with those defining the already existing classes. Each tested vector is assigned to the closest class or defines a new class if it is too far from all existing classes. Once this classification stage is complete, we estimate a unique line for each class by repeating the line parameter estimation procedure described in Part I, but using a new matrix $X(\psi)$ containing all the pixel values corresponding to that class.

[1] These assumptions concern the linear independence of non-zero vectors $\bar{f}_i(\psi)$ and of corresponding shifted mixing matrix columns. These assumptions and the effect of constant sources cannot be detailed here, due to space limitations.

3.2.3. Part III: Computing minimum-distance points between two lines

This last part is the most important one in the identification stage. The coordinates of each endmember (column of the mixing matrix) are derived by estimating the intersection points of two lines corresponding to two pairs of sources. This is feasable under the assumption that there exists a common point between each pair of lines. In theory, this condition is met if the considered two pairs of sources share one source. In practice, however, it is possible that two estimated lines do not exactly intersect due to data noise. In this case, the endmember coordinates may be estimated by computing the minimum-distance points between two lines. Hereafter, we show how to calculate the minimum distance between two lines in an L-dimensional space. This is achieved by finding two points, $\mathbf{p}_{s_C}$ on the line D_1 and $\mathbf{q}_{t_C}$ on another line D_2, where this minimum occurs [21]. D_1 and D_2 are defined respectively by:

$$\mathbf{p}_s = s\mathbf{u}^* + \mathbf{d}^* \text{ and } \mathbf{q}_t = t\mathbf{v}^* + \mathbf{e}^*. \quad (15)$$

w(s,t) $= \mathbf{p}_s - \mathbf{q}_t$ is a given vector between two points on the two lines. We want to find the **w**(s_C, t_C) (hereafter denoted $\mathbf{w}_C$) that has a minimum length among all s and t. To this end, we have to find the line segment $(p_{s_C}\ q_{t_C})$ joining these points and which is simultaneously perpendicular to the two lines D_1 and D_2 [21]. In other words, the vector $\mathbf{w}_C$ is perpendicular to the direction-vectors $\mathbf{u}^*$ and $\mathbf{v}^*$, and this is equivalent to satisfy (1) ${\mathbf{u}^*}^T\mathbf{w}_C = 0$ and (2) ${\mathbf{v}^*}^T\mathbf{w}_C = 0$.
We can easily solve this couple of equations by replacing $\mathbf{w}_C$ by $\mathbf{p}_{s_C} - \mathbf{q}_{t_C}$ (with $\mathbf{w}_0 = \mathbf{d}^* - \mathbf{e}^*$), which yields:

$$\begin{aligned} ({\mathbf{u}^*}^T\mathbf{u}^*)s_C - ({\mathbf{u}^*}^T\mathbf{v}^*)t_C &= -{\mathbf{u}^*}^T\mathbf{w}_0 \\ ({\mathbf{v}^*}^T\mathbf{u}^*)s_C - ({\mathbf{v}^*}^T\mathbf{v}^*)t_C &= -{\mathbf{v}^*}^T\mathbf{w}_0. \end{aligned}$$

Then, by denoting $a_1 = {\mathbf{u}^*}^T\mathbf{u}^*$, $a_2 = {\mathbf{u}^*}^T\mathbf{v}^*$, $a_3 = {\mathbf{v}^*}^T\mathbf{v}^*$, $a_4 = {\mathbf{u}^*}^T\mathbf{w}_0$, and $a_5 = {\mathbf{v}^*}^T\mathbf{w}_0$, we obtain:

$$s_C = \frac{a_3a_4 - a_5a_2}{{a_2}^2 - a_1a_3}, \text{ and } t_C = \frac{a_2a_4 - a_1a_5}{{a_2}^2 - a_1a_3}, \text{ with } {a_2}^2 - a_1a_3 \neq 0.$$

Eq. (15) then yields the points p_{s_C} and q_{t_C} on the two lines D_1 and D_2, where they are the closest to each other. If the minimum distance between the two lines $d(D_1, D_2) = \left\|\mathbf{p}_{s_C} - \mathbf{q}_{t_C}\right\|$ is less than a threshold (experimentally set to 10^{-3} in our tests), the means of the coordinates of $\mathbf{p}_{s_C}$ and $\mathbf{q}_{t_C}$ are retained as one of the columns of the sought mixing matrix. This is repeated for all the other intersection points.

3.3. Extraction stage

After estimating the spectrum of each pure material, we undertake the final part of our method, which consists in extracting the M abundance maps (sources) that are present in the considered data. To this end, we apply the Non-negative Least Squares (NLS) method to each pixel of the considered data [22]. It should be noted that in order to satisfy the sum-to-one constraint defined by Eq. (2), we add to the observation and spectra matrices, a row consisting of a positive constant value [23]. Besides, our overall BSS method is applicable to mixtures which are underdetermined over the complete image ($L < M$), provided these mixtures remain (over)determined in each pixel.

4. TEST RESULTS

To evaluate the performance of our method, we compare the estimated and actual sources using the normalized root mean square error (NRMSE). For the mixing matrix, we use the spectral angle mapper (SAM in degrees). These criteria are defined by:

$$\text{NRMSE (of the sources)} = \frac{\|\text{real - estimated}\|}{\|\text{real}\|}$$
$$\text{SAM (of the mixing matrix)} = \arccos\left(\frac{\langle\text{real,estimated}\rangle}{\|\text{real}\|\cdot\|\text{estimated}\|}\right).$$

A dataset of 8 realistic sources (80×80-pixel abundance fraction maps, cf. Figure 2) was created from a real classification of land cover (see [18] for details). The observed image was generated by linear combinations of these sources (Eq. (1)) and using random spectra composed of four samples (mixing matrix). The used image was also corrupted by an additive white noise (with 60 dB-SNR). We then applied our method to separate these mixtures. Table 1 shows the results obtained using (a) the proposed method and (b) the classical SMACC method [6] (implemented in a standard commercial image processing software). As can be noted, our method yields much better average performance than SMACC, and only SMACC completely fails for some sources (s_3 and s_7).

Table 1. Obtained results using: (a) our method, (b) SMACC

		s_1	s_2	s_3	s_4	s_5	s_6	s_7	s_8	mean
a	NRMSE	0.029	0.016	0.054	0.003	0.019	0.015	0.229	0.009	**0.041**
	SAM	0.014	0.059	0.199	0.099	0.011	0.328	0.817	0.043	**0.174**
b	NRMSE	0.047	0.062	**0.900**	0.026	0.101	0.015	**1.183**	0.075	**0.267**
	SAM	0.103	0.112	**12.51**	0.021	0.079	0.079	**11.48**	0.081	**2.719**

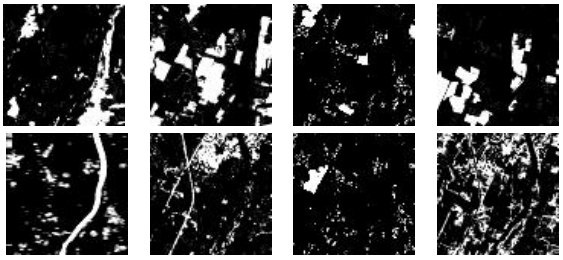

Fig. 2. The eight realistic sources used in our tests

5. CONCLUSION AND FUTURE WORK

In this paper, we proposed a new unsupervised BSS approach based on spatial sparsity for multispectral images. The proposed approach consists of three stages: (i) determining all the two-source zones present in the considered data using a correlation-based detector, (ii) identifying the columns of the mixing matrix from the intersections of the lines generated by the two-source zones, and finally (iii) reconstructing the searched sources using a non-negative least squares method. We experimentally validated the effectiveness of our method using simulated mixtures of realistic sources and we obtained very attractive results. Our future investigations will be devoted to extending our method to spatial unmixing of hyperspectral images. Other classification and two-source zone detection methods will also be explored.

6. REFERENCES

[1] J.M. Bioucas-Dias, A. Plaza, N. Dobigeon, M. Parente, Q. Du, P. Gader, and J. Chanussot, "Hyperspectral unmixing overview: Geometrical, statistical, and sparse regression-based approaches," *IEEE J. of Sel. Topics in Appl. Earth Observ. Remote Sens.*, vol. 5, no. 2, pp. 354–379, April 2012.

[2] N. Keshava and J.F. Mustard, "Spectral unmixing," *IEEE Signal Processing Magazine*, vol. 19, no. 1, pp. 44–57, January 2002.

[3] P. Comon and C. Jutten, *Handbook of Blind Source Separation: Independent Component Analysis and Applications*, Academic Press, 2010.

[4] A. Hyvarinen, J. Karhunen, and E. Oja, *Independent Component Analysis*, John Wiley and Sons, 2001.

[5] A. Cichocki, R. Zdunek, A. H. Phan, and S-I. Amari, *Nonnegative Matrix and Tensor Factorizations: Applications to Exploratory Multi-way Data Analysis and Blind Source Separation*, John Wiley and Sons, Chichester, United Kingdom, 2009.

[6] J. Gruninger, A.J. Ratkowski, and M.L. Hoke, "The sequential maximum angle convex cone (smacc) endmember model," in *Algorithms for Multispectral, Hyperspectral and Ultraspectral Imagery*. SPIE, 2004, vol. 5425, no. 1.

[7] J. Gruninger, A.J. Ratkowski, and M.L. Hoke, "The extension of endmember extraction to multispectral scenes," in *Algorithms for Multispectral, Hyperspectral and Ultraspectral Imagery*. SPIE, 2004, vol. 5425, no. 2.

[8] S. Bernab, P.R. Marpu, A. Plaza, and J.A. Benediktsson, "Spectral unmixing of multispectral satellite images with dimensionality expansion using morphological profiles," in *Satellite Data Compression, Communications, and Processing VIII*. SPIE, 2012, vol. 8514.

[9] A. Ifarragurri and C-I. Chang, "Multispectral and hyperspectral image analysis with convex cones," *IEEE Trans. on Geoscience and Remote Sensing*, vol. 37, no. 2, pp. 756–770, March 1999.

[10] A. Zare, P. Gader, O. Bchir, and H. Frigui, "Piecewise convex multiple-model endmember detection and spectral unmixing," *IEEE Trans. on Geoscience and Remote Sensing*, vol. 51, no. 5, pp. 2853–2862, May 2013.

[11] A. Jourjine, S. Rickard, and O. Yilmaz, "Blind separation of disjoint orthogonal signals: Demixing n sources from 2 mixtures," in *Int. Conf. Acoustics, Speech, Signal Processing (ICASSP)*. IEEE, 2000, vol. 5, pp. 2985–2988.

[12] O. Yilmaz and S. Rickard, "Blind separation of speech mixtures via time-frequency masking," *IEEE Trans. on Signal Processing*, vol. 52, no. 7, pp. 1830–1847, July 2004.

[13] P. Georgiev, F. Theis, and A. Cichocki, "Sparse component analysis and blind source separation of underdetermined mixtures," *IEEE Trans. Neural Networks*, vol. 16, no. 4, pp. 992–996, July 2005.

[14] Y. Li, S-I. Amari, A. Cichocki, D.W.C Ho, and S. Xie, "Underdetermined blind source separation based on sparse representation," *IEEE Trans. on Signal Processing*, vol. 54, no. 2, pp. 423–437, February 2006.

[15] Y. Deville and M. Puigt, "Temporal and time-frequency correlation-based blind source separation methods. part i: determined and underdetermined linear instantaneous mixtures," *Signal Processing*, vol. 87, no. 3, pp. 374–407, March 2007.

[16] F. Abrard and Y. Deville, "A time-frequency blind signal separation method applicable to underdetermined mixtures of dependent sources," *Signal Processing*, vol. 85, no. 7, pp. 1389–1403, July 2005.

[17] Y. Deville, D. Bissessur, M. Puigt, S. Hosseini, and H. Carfantan, "A time-scale correlation-based blind separation method applicable to correlated sources," in *ESANN*. European Symposium on Artificial Neural Networks, 2006, pp. 337–343.

[18] M.S. Karoui, Y. Deville, S. Hosseini, and A. Ouamri, "Blind spatial unmixing of multispectral images: New methods combining sparse component analysis, clustering and nonnegativity constraints," *Pattern Recognition*, vol. 45, no. 12, pp. 4263–4278, December 2012.

[19] S. Wold, "Principal component analysis," *Chemometrics and Intelligent Laboratory Systems*, vol. 2, no. 1-3, pp. 37–52, August 1987.

[20] A. Smilde, R. Bro, and P. Geladi, *Multi-way analysis with applications in the chemical sciences*, John Wiley and Sons, England, 2004.

[21] P.J. Schneider and D.H. Eberly, *Geometric Tools for Computer Graphics*, Elsevier Science, USA, 2003.

[22] C.L. Lawson and R.J. Hanson, *Solving Least Squares Problems*, Society for Industrial and Applied Mathematics, 1995.

[23] D.C. Heinz and C.I. Chang, "Fully constrained least squares linear spectral mixture analysis method for material quantification in hyperspectral imagery," *IEEE Trans. on Geoscience and Remote Sensing*, vol. 39, no. 3, pp. 529–545, March 2001.